THE JOURNAL OF PHYSICAL CHEMISTRY A

ARTICLE

pubs.acs.org/JPCA

# Path Integral Monte Carlo Study of $^4$He Clusters Doped with Alkali and Alkali-Earth Ions

D. E. Galli,*,† D. M. Ceperley,‡ and L. Reatto†

†Dipartimento di Fisica, Università degli Studi di Milano, via Celoria 16, 20133 Milano, Italy

‡Department of Physics, University of Illinois at Urbana−Champaign, Urbana, Illinois 61801, United States

**ABSTRACT:** Path integral Monte Carlo calculations of $^4$He nanodroplets doped with alkali ($Na^+$, $K^+$ and $Cs^+$) and alkali-earth ($Be^+$ and $Mg^+$) ions are presented. We study the system at $T$ = 1 K and between 14 and 128 $^4$He atoms. For all studied systems, we find that the ion is well localized at the center of the droplet with the formation of a "snowball" of well-defined shells of localized $^4$He atoms forming solid-like order in at least the first surrounding shell. The number of surrounding helium shells (two or three) and the number of atoms per shell and the degree of localization of the helium atoms are sensitive to the type of ion. The number of $^4$He atoms in the first shell varies from 12 for $Na^+$ to 18 for $Mg^+$ and depends weakly on the size of the droplet. The study of the density profile and of the angular correlations shows that the local solid-like order is more pronounced for the alkali ions with $Na^+$ giving a very stable icosahedral order extending up to three shells.

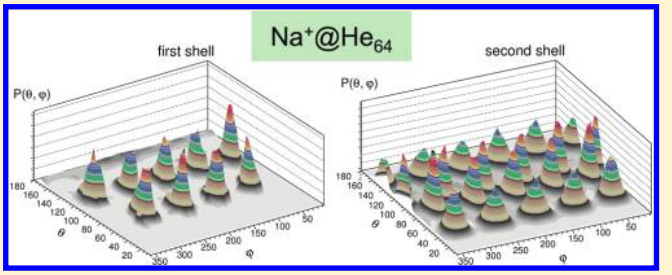


## INTRODUCTION

Nanodroplets of $^4$He as nanorefrigerators to study molecules are widely used in physics and in chemistry. The way was paved by the pioneering works by Toennies and collaborators[1] and by Scoles and collaborators.[2] In the past few years, positive ions in nanodroplets of $^4$He have also been studied experimentally.[3−9] Actually, the study of charged particles in bulk $^4$He has a long history as one of the first microscopic probes that have been used to study such a superfluid system.[10,11] Negatively charged impurities such as an electron or a $He^-$ ion are believed to form a microscopic bubble in liquid $^4$He due to the repulsion that arises from the Pauli exclusion principle between the electrons of the neutral atoms and those of the charged particle. By contrast, the local density around a positive ion is expected to increase due to electrostriction. Using a phenomenological estimate, the local density turns out to be so large that $^4$He should solidify around the ion. This is the "snowball model" developed by Atkins[12] and widely used in the interpretation of the earlier experiments of ions in bulk superfluid $^4$He. A similar snowball is expected to be present also if the ion is captured inside a droplet of He. Recent experiments of ions such as $Ag^+$, $Mg^+$, $Rb^+$, $Na^+$, $K^+$, $Cs^+$, as well as $Pb^+$, $Cd^+$, $Zn^+$, $F^+$, $Cl^+$, $Br^+$, and $I^+$ have been discussed in terms of the formation of a snowball.[3−9] The first microscopic treatment of a positive alkali ion in bulk and in nanodroplets of $^4$He was performed about 10 years ago. Such studies have been performed at $T$ = 0 K by an advanced variational theory based on the shadow wave function (SWF) and by a variant of it, the so-called glue-SWF, that allows one to also treat nanodroplets of $^4$He.[13−15] This variational theory confirmed the formation of a snowball around the ion with the formation of well-defined shells of $^4$He atoms. The major result of those computations is that the size of the snowball, the number of atoms in the shells, and the kind of local order depend on the specific ion. This behavior is completely different from that given by the Atkins' model: his snowball only depends on the ionic charge. The presence of magic numbers for the closure of the shells is supported by recent experiments, and good agreement between theory and experiment was found when comparison has been possible.[7]

The attractive interaction between a $^4$He atom and a positive ion is much larger than the He−He interaction; this represents a challenge to any microscopic theory. For example, in the variational theory it was found[15] very important to allow anisotropic correlations for the radial ion−He motion, since this directly probes the ion−He potential. This is in contrast to the tangential motion, which mainly probes the He−He potential. It is important to go beyond the limitations of the variational approach in order to get unbiased results. This motivates the present work in which we have studied some of the alkali and of the alkali-earth ions in nanodroplets of $^4$He at finite temperature by the path integral Monte Carlo (PIMC) methods.[16] PIMC has been already applied to the study of a $Na^+$ ion in a $^4$He droplet.[17] That study gave a snowball structure quite different from the glue-SWF result and in disagreement with later quantum Monte Carlo calculations with the path integral ground state (PIGS) method.[18] Here we revisit this system, and additionally we study $K^+$, $Cs^+$, $Be^+$, and $Mg^+$. Both the $^4$He atoms and the ions are

**Special Issue:** J. Peter Toennies Festschrift

**Received:** January 20, 2011
**Revised:** May 13, 2011
**Published:** May 15, 2011

treated at a full quantum level using Bose statistics for the $^4$He atoms. We study the energetics, the local correlations, the degree of localization, and the local solid-like order. We confirm that the ions reside at the center of the droplet for the sizes we have studied, from 14 up to 128 $^4$He atoms. Overall, the PIMC results confirm those of the glue-SWF[15] with only minor deviations. We notice that extensive studies of alkali ions in very small clusters of $^4$He have been performed by Gianturco and collaborators[19−21] with the diffusion Monte Carlo method.

The organization of the paper is as follows: In Section II we give the Hamiltonian and some details on our PIMC computation, and in Section III we present the results and the discussion. The conclusions are contained in Section IV.

## SIMULATION DETAILS

The PIMC is a method to calculate the thermodynamic properties of a quantum system at finite temperature, based on Feynman's original idea of mapping path integrals onto a type of interacting classical ring−polymers. When applied to quantum systems of bosons, PIMC can provide exact estimates for properties, within the statistical uncertainties of the Monte Carlo calculation and other controlled errors. For the clusters considered here, the only uncontrolled error is the assumed interatomic potential. The PIMC method has been successfully applied to bulk liquid helium, and to droplets of pure helium and para-hydrogen molecules. A detailed review of this method is given in ref 16, together with a review of results on bulk helium. The many-body density matrix at a temperature $T$ is

$$\rho(R, R'; \beta) = \langle R|e^{-\beta \hat{H}}|R'\rangle \quad (1)$$

where $\beta = 1/k_B T$, $\hat{H}$ is the Hamiltonian of an $N$-body system, and $R$ represents a $3N$-dimensional vector of coordinates, $R = \{\vec{r}_1, \vec{r}_2, ..., \vec{r}_N\}$. The thermal average of an operator $\hat{O}$ is given by

$$\langle \hat{O} \rangle = \frac{1}{Z} \int dR\, dR' \langle R|\hat{O}|R'\rangle \rho(R, R'; \beta) \quad (2)$$

where $Z = \int dR \rho(R,R;\beta)$ is the partition function. The low temperature density matrix is not known, but we can represent it with a product (in the coordinate representation by a convolution) of $M$ density matrices at higher-temperature $MT = M/k_B\beta = 1/k_B\tau$:

$$\rho(R, R'; \beta) = \int ... \int dR_1\, dR_2 ... dR_{M-1} \rho(R, R_1; \tau)\rho(R_1, R_2; \tau)...\rho(R_{M-1}, R'; \tau) \quad (3)$$

For a Bose system, the density matrix should be symmetrized; this is accomplished by summing over all permutations $P$ of the particle labels:

$$\rho(R, R'; \beta) = \frac{1}{N!} \sum_P \rho(R, PR'; \beta) \quad (4)$$

In the present quantum calculations, we used $MT = 1/k_B\tau = 160$ K for the high−temperature density−matrix $\rho(R,R';\tau)$; this was sufficient to obtain converged results within the pair-product approximation.[16] In order to calculate the multidimensional integral of eq 2, coupled with eq 3 and eq 4, we employ a generalized Metropolis algorithm which includes both spatial and permutational moves; details can be found in ref 16. The average of an operator $\hat{O}$ can be determined simply by taking the average of $\langle R|\hat{O}|R'\rangle$ over the sampled paths. In our PIMC simulations, in addition to the $N$ $^4$He atoms, we have one ion. The ion is also treated quantum mechanically.

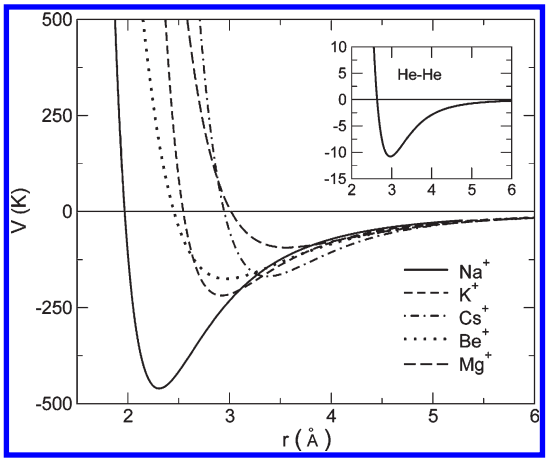


**Figure 1.** The ion−helium interaction potentials,[22−24] compared with the He−He interaction potential,[25] which is shown in the inset.

For the potential energy, we use the sum of pair potentials between helium atoms and between the ion and any helium atom. Therefore, we have the following system Hamiltonian:

$$\hat{H} = -\frac{\hbar^2}{2m_4} \sum_{i=1}^{N} \nabla_i^2 - \frac{\hbar^2}{2m_I} \nabla_I^2 + \sum_{i<j} v(|\vec{r}_i - \vec{r}_j|) + \sum_i^N V_I(|\vec{r}_I - \vec{r}_i|) \quad (5)$$

where $m_4$ is the mass of a helium atom, $m_I$ is the mass of the ion, $v(r)$ is the helium−helium interaction potential, and $V_I(r)$ is the ion−helium interaction. We have described the ion−helium interaction by accurate model potentials developed in the literature;[22−24] For the helium−helium interaction we have chosen a well-tested Aziz potential.[25] All the interactions are short-ranged. In order to make a table for the density matrix,[16] we truncate all potentials smoothly at a certain distance $r_c$ using

$$v'(r) = \begin{cases} v(r) - v(r_c) & r \le r_c \\ 0 & r > r_c \end{cases} \quad (6)$$

and a similar expression for $V_I'(r)$. The cutoff radius has been fixed to 8 Å for all interactions. The quantum simulations are performed with the potentials $v'(r)$ and $V_I'(r)$. The resulting potential and total energies are corrected by a tail contribution, $\Delta V$, that is obtained by averaging the missing potential energy $\Sigma_{i<j}\delta v(|\vec{r}_i - \vec{r}_j|) + \Sigma_i \delta V_I(|\vec{r}_I - \vec{r}_i|)$, where $\delta v = v - v'$ and $\delta V_I = V_I - V_I'$. $\Delta V$ can be computed in terms of the density profile, $\rho(r)$, around the ion and of the average pair correlation function, $g(r)$, giving the probability of finding two He atoms at distance $r$.

We have not added any artificial confinement potential to prevent the helium atoms from evaporating because the binding of the $^4$He atoms to the ion prevents such evaporation. In Figure 1 we plot the relevant interaction potentials; we notice that the ion−helium potentials have a very deep attractive well, as compared with the He−He potential. The well of the potential and the location of its minimum strongly depends on the specific ion; for example, in the $Na^+$−$^4$He case,[22] the most attractive, the well is about −445 K deep, and the minimum is located at about 2.3 Å, while in the $Mg^+$−$^4$He case,[24] the less attractive, the well is


dx.doi.org/10.1021/jp200617a |J. Phys. Chem. A 2011, 115, 7300–7309

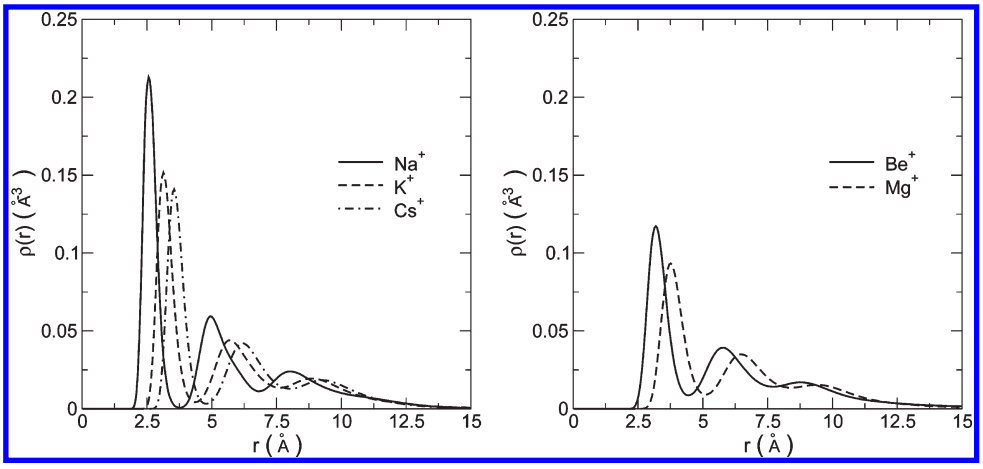


**Figure 2.** Radial $^4$He density, $\rho(r)$, around ions for the largest $^4$He droplets studied in this work: number of atoms $N = 128$.

about −94 K deep with the minimum at about 3.6 Å. This strong ion−He interaction produces the clustering of helium atoms around the impurity ion. Notice also that the position of the minimum in the $K^+-{}^4He$ potential[22] is similar to that in $Be^+-{}^4He$,[24] and the same happens comparing the $Cs^+-{}^4He$[23] potential with the $Mg^+-{}^4He$ one;[24] the potential wells between $^4$He and alkali-earth ions, however, are considerably wider because $V_I(r)$ for the alkali-earth ion is less steep at short distance compared to those of the alkali ions.

Under the influence of the ion electric field the He atoms become polarized so that, in principle, the He−He interaction potential is modified for atoms close to the ion; simple estimates based on the polarizability of the He atoms show that this is a small effect and we have neglected it. We have done the majority of the PIMC calculations for the ion−$^4$He droplets at $T = 1$ K. We have performed some calculation also at $T = 0.5$ K, but no significant effect on the properties under study has been found.

We recall that a PIMC calculation consists of a simulation of special interacting ring−polymers, one for each atom in the system; the monomers, which form the ring−polymer associated with a particular atom, correspond to the positions visited by that atom along the path in eq 3. In a typical simulation, at least $10^5$ Monte Carlo steps have been performed; one Monte Carlo step consists of an attempted rigid displacement move of each polymer and of a fixed number (typically $10^3$) of other attempted moves: these were either intrapolymer moves or permutation moves among up to four polymers;[16] the number of monomers affected by such moves was 15, corresponding to four levels in the bisection algorithm. The acceptance ratio for permutation moves was found to increase with the number of $^4$He atoms in the nanodroplet, and the typical acceptance ratio for permutation moves in nanodroplets with $N = 128$ $^4$He atoms was about 2% for two atoms, 1% for three atoms, and 0.5% for a four-atom permutation move. In order to check that the final statistics represent equilibrium, for each studied condition a series of simulations was performed, restarting each simulation from the last configuration of the previous one. Data blocking was used to estimate statistical uncertainties.

## RESULTS AND DISCUSSION

The primary quantities studied in our PIMC calculations are radial density profiles, $\rho(r)$, of $^4$He atoms around the different ions. In Figure 2 we show the density profiles for doped $^4$He droplets with $N = 128$ at $T = 1$ K. The microscopic structure of the snowball is strongly dependent on the identity of the ion: each one produces distinctive modulations (shells) in the helium density. The shells around alkali ions are the most pronounced (sharper and higher), whereas the modulations around the alkali-earth ions have less structure; this is presumably due to the core of the potential which is steepest in the alkali case. As a consequence, the attractive well of the ion−He potential is much narrower in the case of the alkali than in the alkali-earth one. In all cases, the local density of the first shell is well above the freezing density of bulk $^4$He ($\rho_{freeze}$0.0258 Å$^{-3}$), so that some kind of solid order is expected; the local density in the second shell around $Na^+$ is still well above the freezing density, and its shape suggests an underlying local solid structure. However, the density profile by itself is not enough to establish whether such local solid order is indeed present and the degree of localization of the He atoms. For this a more elaborate analysis is needed, as discussed below. Such analysis will show that what appears sometimes as a unique peak in the density profile corresponds to two shells of atoms with overlapping densities. From Figure 2, it can also be noticed that the minimum between the first and the second peak is lower for the alkali than for the alkali-earth ions. This suggests, and this we shall prove later, that the $^4$He atoms in the snowball of an alkali-earth ion can exchange more easily between the first and the second shell.

In Table 1 we show the total, kinetic, and potential energies computed in doped nanodroplets of different sizes. The energies reported in Table 1 include the tail corrections due to the truncation of the potentials. In this table the position, $r_P$, of the peak of the first shell, the value of the distance from the ion, $r_1$, where the density profiles show a minimum between the first and the second shell is also shown; by numerical integration of the density profile up to $r_1$, we have obtained the average number of atoms in the first shell, $N_1$, around the ion. $N_1$ turns out to depend not only on the particular ion inside the nanodroplet but it has also a weak dependence on the number of $^4$He atoms of the droplet. The only exception to this last observation is found for nanodroplets doped with $Na^+$, that have, in the range $N = 32-128$ $^4$He atoms, a remarkable stability in the value of $N_1$.

In order to clarify the role of statistics in these systems, we have also performed PIMC simulations of doped nanodroplets without sampling permutations among $^4$He atoms, i.e., for

**Table 1. Total $E/N$, Kinetic $K/N$ and Potential $V/N$ Energies Per Particle of Alkali and Alkali-Earth $^4$He-Doped Nanodroplets with Different Number, $N$, of $^4$He Atoms at $T = 1$ K. The peak position of the first shell, $r_P$, the position, $r_1$, of the minimum in the density profiles between the first and the second shell together with the number of $^4$He, $N_1 = N(r_1)$, within a sphere of radius $r_1$ around the ion are also shown.**

| ion | $N$ | $E/N$ (K) | $K/N$ (K) | $V/N$ (K) | $r_P$ (Å) | $r_1$ (Å) | $N_1$ |
|---|---|---|---|---|---|---|---|
| $Na^+$ | 32 | −108.38 ± 0.28 | 42.81 ± 0.37 | −151.19 ± 0.28 | 2.58 | 3.82 | 11.99 ± 0.01 |
| $Na^+$ | 64 | −60.17 ± 0.09 | 29.50 ± 0.17 | −89.67 ± 0.16 | 2.57 | 3.78 | 12.00 ± 0.01 |
| $Na^+$ | 128 | −34.03 ± 0.12 | 19.86 ± 0.20 | −53.89 ± 0.10 | 2.57 | 3.78 | 12.00 ± 0.01 |
| $K^+$ | 32 | −68.28 ± 0.06 | 30.81 ± 0.06 | −99.09 ± 0.06 | 3.12 | 4.31 | 14.08 ± 0.04 |
| $K^+$ | 64 | −39.83 ± 0.05 | 23.53 ± 0.09 | −63.36 ± 0.08 | 3.11 | 4.28 | 14.05 ± 0.04 |
| $K^+$ | 128 | −23.53 ± 0.09 | 17.02 ± 0.11 | −40.55 ± 0.09 | 3.14 | 4.36 | 15.00 ± 0.05 |
| $Cs^+$ | 32 | −64.62 ± 0.06 | 29.72 ± 0.09 | −94.34 ± 0.06 | 3.53 | 4.75 | 17.1 ± 0.1 |
| $Cs^+$ | 64 | −37.91 ± 0.05 | 23.11 ± 0.09 | −61.02 ± 0.08 | 3.55 | 4.80 | 17.9 ± 0.2 |
| $Cs^+$ | 128 | −22.90 ± 0.06 | 16.58 ± 0.07 | −39.48 ± 0.05 | 3.55 | 4.79 | 18.0 ± 0.1 |
| $Be^+$ | 32 | −60.53 ± 0.06 | 28.63 ± 0.16 | −89.16 ± 0.09 | 3.16 | 4.44 | 14.3 ± 0.2 |
| $Be^+$ | 64 | −35.95 ± 0.05 | 22.05 ± 0.13 | −58.00 ± 0.09 | 3.18 | 4.43 | 14.8 ± 0.2 |
| $Be^+$ | 128 | −21.94 ± 0.05 | 15.84 ± 0.07 | −37.78 ± 0.11 | 3.19 | 4.44 | 15.0 ± 0.1 |
| $Mg^+$ | 32 | −38.78 ± 0.06 | 21.09 ± 0.09 | −59.87 ± 0.09 | 3.76 | 5.25 | 18.2 ± 0.2 |
| $Mg^+$ | 64 | −25.37 ± 0.04 | 17.75 ± 0.08 | −43.12 ± 0.09 | 3.75 | 5.11 | 18.2 ± 0.2 |
| $Mg^+$ | 128 | −16.07 ± 0.05 | 13.98 ± 0.11 | −30.05 ± 0.09 | 3.76 | 5.10 | 18.4 ± 0.2 |

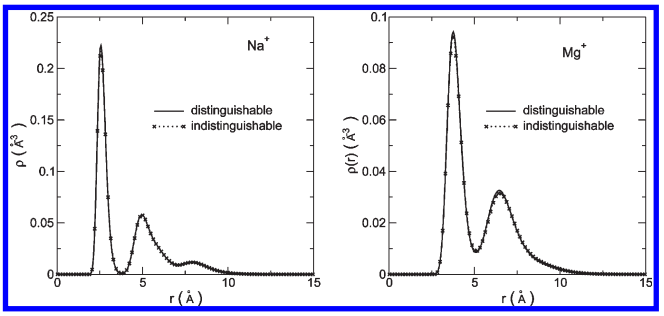


**Figure 3.** Radial $^4$He densities $\rho(r)$ around a $Na^+$ ion and a $Mg^+$ ion in droplets with $N = 64$ $^4$He atoms with and without the sampling of permutations among $^4$He atoms.

distinguishable $^4$He atoms. We considered only droplets with $N = 64$ atoms. The density profiles around the ion, $\rho(r)$, the peak position of the first shell, $r_P$, the position, $r_1$, of the minimum in the density profiles between the first and the second shell, and the number of $^4$He, $N_1 = N(r_1)$, within a sphere of radius $r_1$ around the ion turn out to be very similar to the values found with indistinguishable $^4$He atoms. In Figure 3 we show the density profiles computed with and without permutations, for nanodroplets doped with $Na^+$ and $Mg^+$ at $T = 1$ K. The kinetic energies computed in the simulations (with $N = 64$) for distinguishable $^4$He atoms turned out to be higher than the value found in the simulations where the Bose statistics was used. Moreover, potential energies turned out to be more negative but to a smaller extent, giving an overall increase of the total energies in these systems. For example, for $Na^+$, the kinetic energy per particle increases by about 0.8 K, and the potential energy decreases by about 0.4 K; for $Mg^+$, the increase in the kinetic energy per particle is about 0.9 K, and the decrease of the potential energy per particle is about 0.5 K. Considering the statistical uncertainties in Table 1, it turns out that the effect of the statistics on the energies is sizable. This effect is reasonable because distinguishable atoms are more localized than indistinguishable ones.

We now discuss the structure of the snowball around each alkaline or alkaline-earth ions that we studied, starting from the $Na^+$ case.

**$Na^+$-Doped Nanodroplets.** The $Na^+$ ion gives rise to a very sharp modulation of the density peaks, due to a particular matching of the ion's size with the shape of the ion−He and He−He potentials. By a numerical integration of the density profiles, we obtain the number of $^4$He atoms, $N(r)$, within a sphere of radius $r$ centered around the ion. In Figure 4 we show the density profiles computed at $T = 1$ K for different number, $N$, of $^4$He atoms together with $N(r)$ for the same nanodroplets. We found that the number of He atoms in the first shell around this ion, $N_1$, is 12 when the number of He atoms in the nanodroplets is more than 30, but it is 10 for smaller nanodroplets; in Figure 4 the density profile and $N(r)$ for a nanodroplet with $N = 20$ are shown as an example. The value $N_1 = 12$ is in agreement with other quantum Monte Carlo studies of ion-doped nanodroplets, based on an accurate SWF variational technique,[15] and with the exact PIGS method[18] both are zero temperature techniques. By integration of the density profile in the region of the second maximum, one finds about 32 He atoms. One can notice in Figure 4 that this maximum is rather asymmetric, and in fact, as shown from an angular correlation function analyzed below, this second maximum represents the overlap of two different shells.

In order to obtain information on the radial localization of $^4$He atoms around the ion, one can map the Monte Carlo evolution of the distance between an helium atom and the ion during the simulation run. This is shown in Figure 5a where the radial positions of three $^4$He atoms started at different radial distances in a cluster of 64 $^4$He atoms at $T = 1$ K are followed for $10^4$ Monte Carlo steps. What is shown is the evolution of the distances between some helium coordinates and the ion coordinate at a fixed time-slice, one of the $M$ time-slices that characterize the polymers in our simulation; this means that when these distances change, the changes can be attributed either to a Monte Carlo move of the ion or the $^4$He atom or both, or an exchange move that has swapped one helium atom into another one. As shown in Figure 5a, we find that atoms started at a particular radial position

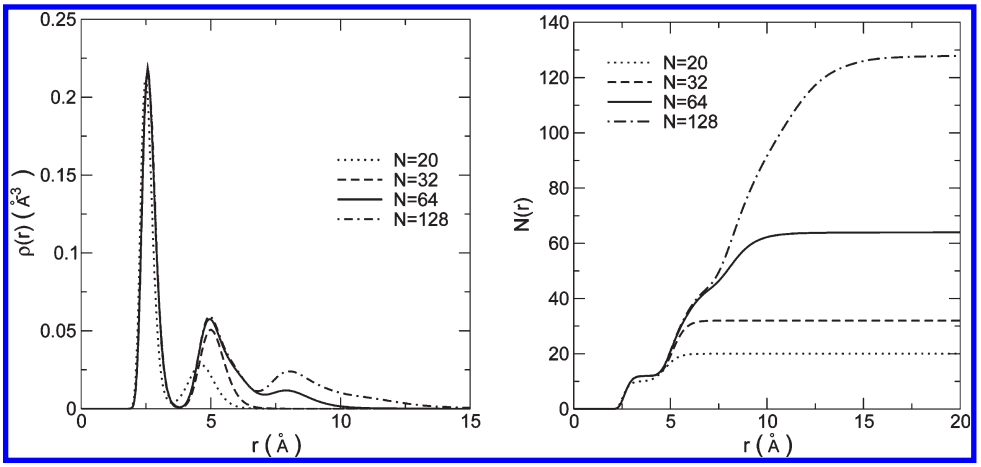


**Figure 4.** Radial $^4$He density $\rho(r)$ and number of atoms $N(r)$ within a sphere of radius $r$ around a $Na^+$ ion for droplets with different number, $N$, of $^4$He atoms.

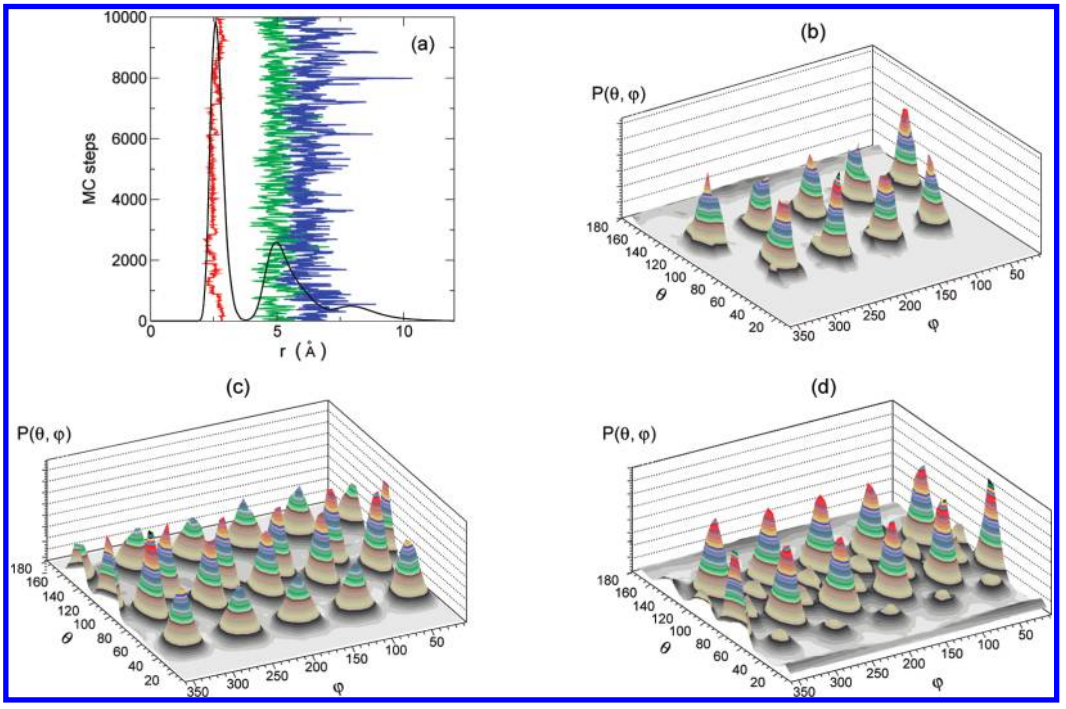


**Figure 5.** (a) Monte Carlo evolution of the distance of three $^4$He atoms from a $Na^+$ ion, started at different radial distances from the ion in a droplet with $N = 64$ $^4$He atoms. The radial density profile (black) in arbitrary units is also shown. The distance is monitored at a fixed time-slice. (b,c,d) Angular correlations, $P(\theta,\varphi)$, among $^4$He atoms inside spherical shells around a $Na^+$ ion in a $^4$He droplet with $N = 64$ $^4$He atoms: $\theta \in [60°,78°]$ (b) $r \leq 3.78$ Å (c) 3.78 Å $< r \leq 5.37$ Å (d) 5.37 Å $< r \leq 7.03$ Å .

in the first ($r \leq 3.78$ Å) or in the second (3.78 Å $< r \leq 7.03$ Å) peak of the density profile, hardly change their radial position, continuing to fluctuate around their starting values. Note that the two atoms in the second peak, one chosen in the inner part of the second peak and one in the outer part, continue to remain near their starting positions. The behavior shown in Figure 5a indicates two things: one is that we expect local solid order both in the first and in the second peak of the density profile, the other is that the second peak could be composed of two different solid shells. It should be noticed that although we expect that all the He atoms move from one shell to another if the MC dynamics is followed for long enough Monte Carlo time, but with a frequency that depends on the specific ion and on the specific shell.

The study of the local density is not enough to determine whether order is present in these shells. As some of us did in the analysis of SWF simulations,[13,15] we have carried out an analysis in terms of the angular correlations within a given shell by introducing an angular probability distribution $P(\theta,\varphi)$ that is derived from a four-body correlation function of the ion and three $^4$He atoms .[13] The ion is set at the origin of the coordinates, and the He atoms that lie in a chosen radial interval, $r \in [r_{min},r_{max}]$, are selected. One of the selected He atom is used to define the $z$ axis, and the position of a second atom defines the $xz$ plane if the angle $\theta$ that it forms with the first He atom and the ion lies in a chosen angular interval $\theta \in [\theta_{min},\theta_{max}]$. $P(\theta,\varphi)$ gives the probability to find a third He atom at angular coordinates $\theta$

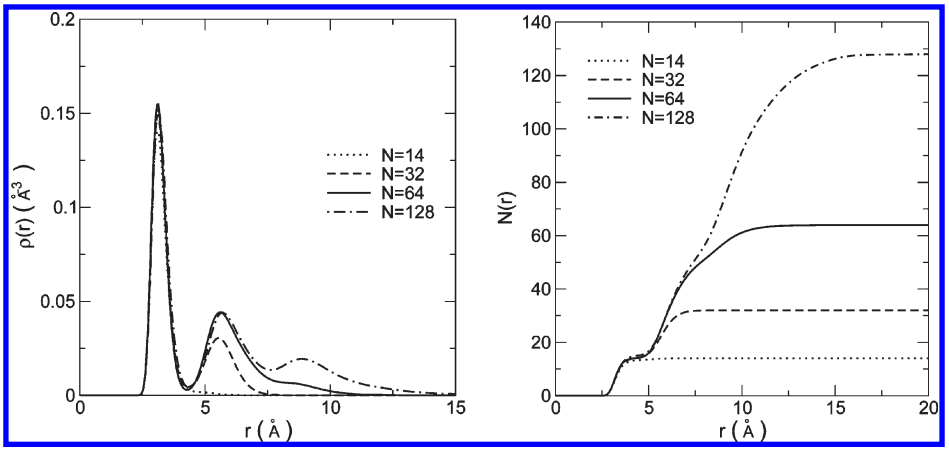


**Figure 6.** Radial $^4$He density $\rho(r)$ and number of atoms $N(r)$ within a sphere of radius $r$ around a $K^+$ ion for droplets with different number, $N$, of $^4$He atoms.

and $\varphi$. When the interval $[r_{min},r_{max}]$ encompasses the first maximum of the density profile, for all the ions considered, $P(\theta,\varphi)$ has modulations extending over the full range of $\theta$ and $\varphi$, revealing the existence of solid-like order in the first shell. This order turns out to be specific to the impurity ion and the result for the $Na^+$ case is shown in Figure 5b for a nanodroplet with $N = 64$ $^4$He atoms at $T = 1$ K. In Figure 5b the angular correlations among $^4$He atoms in the first shell are shown. The actual number of peaks one can see in Figure 5b, 9, is smaller than the number of atoms of the first shell ($N_1 = 12$). One has to take into account that two He atoms that have been used to define the $z$ axis and the $xz$ plane do not appear in the plots of $P(\theta,\varphi)$. In addition, if there is a particle along the $z$ axis ($\theta = 180°$), it hardly shows up in the plot, since its peak is distributed over all $\varphi$ angles. Taking into account these remarks, there is agreement between the value $N_1 = 12$ found by integrating $\rho(r)$ in the first shell and the analysis of the angular correlations. By considering all the ions, the position of the peak of the first shell is about 3 Å; having the ion at the origin of the axes and one atom of the first shell on the $z$ axis, it turns out that another $^4$He atom in the first shell and at $\theta = 60°$ would form an equilateral triangle with the previous two particles. Near freezing, the first maximum in the radial distribution function of bulk $^4$He is found at about 3.4 Å; thus we have considered $\theta_{min} = 60°$ as a lower limit to find the $^4$He atom, nearest neighbor of the one on the $z$ axis, that defines the $xz$ plane; $\theta_{max} = 78°$ has been chosen in order to take ~3.7 Å as the maximum distance where one finds a nearest neighbor in the first shell. This motivates our choice of $\theta_{min} = 60°$ and $\theta_{max} = 78°$ in computing $P(\theta,\varphi)$. The value $N_1 = 12$ is compatible with a Platonic solid, and in fact the angles $\theta$ and $\varphi$ of the peaks in Figure 5b correspond to those expected for an icosahedron as found previously with the SWF technique[15] but also later with the PIGS method.[18]

The angular analysis has been extended to the He atoms outside the first shell in different ways. In order to show whether atoms in the outer shells are correlated with the ones in the first shell, we study a cross correlation: the position of the ion and of two $^4$He atoms of the first shell are used to define the $z$ axis and the $xz$ plane as discussed above. We then compute the probability $P(\theta,\varphi)$ of finding a third He atom at angular position $\theta$ and $\varphi$ and within a given radial distance corresponding to an outer shell. By trial and error we have fixed the interval for the second shell (3.78 Å < $r \leq$ 5.37 Å) and for the third shell (5.37 Å < $r \leq$ 7.03 Å), which both belong to the second peak of the density profile. These angular correlation are shown in Figure 5c for the second shell, and in Figure 5d for the third shell. Well-defined peaks are present, so we conclude that atoms in the second and in the third shell around the ion $Na^+$ also exhibit angular order. Furthermore, the angular probability distributions reveal that the outer shells are angularly correlated to the first shell. In particular, we notice that the outer atoms tend to fill in the space left available by the inner atoms, so that the resulting structure is more compact: the second solid shell is compatible with a dodecahedron (20 $^4$He atoms) while the third solid shell is compatible with a icosahedron. Note that because the two $^4$He atoms which define the $z$ axis and the $xz$ plane belong to the first shell, all the atoms in the second and in the third shells show up as peaks in $P(\theta,\varphi)$ except for those atoms at $\theta = 0$ and at $\theta = 180°$, since, again those peaks are distributed over all $\varphi$ angles. In Figure 5c,d, one can see the presence of some very weak peaks in addition to the main ones. Such weak peaks are due to the spilling of atoms from the second shell into the third one or vice versa.

A PIMC simulation of the $Na^+$—$^4$He system ($N = 30 - 100$ $^4$He atoms) has been performed some time ago[17] using a different $Na^+$—$^4$He potential. They find a shell structure within the snowball, but these results are different from ours, for instance they find 16 He atoms in the first shell instead of 12. This is probably due to the time-step used in the approximated density-matrix which was not small enough, $MT = 1/k_B\tau = 20$ K, as already suggested in ref 18, so that the full quantum nature of the helium atoms were not taken into account.

We conclude that the snowball formed by $Na^+$ is particularly stable and ordered with the presence of three shells of $^4$He atoms with a sequence of icosahedral, dodecahedral, and icosahedral order. Therefore we expect that $Na^+$ in nanodroplets of $^4$He atoms will show the most pronounced magic shell effects among the ions studied in the present paper.

**$K^+$-Doped Nanodroplets.** In Figure 6 the density profiles of some helium nonodroplets doped with a $K^+$ ion for different numbers, $N$, of $^4$He atoms are shown. The density profile for the case $N = 14$ consists of a single radial density peak with a small tail at larger distances. The integration of the density profile for $N = 14$ indicates that the peak is formed from 13 $^4$He atoms, and the tail is due to a single atom outside this shell. By increasing the number of $^4$He atoms in the nanodroplets, a well-defined second modulation in the density profile appears, and the first shell consists of 14—15 $^4$He atoms, going from $N = 32$ to $N = 128$.

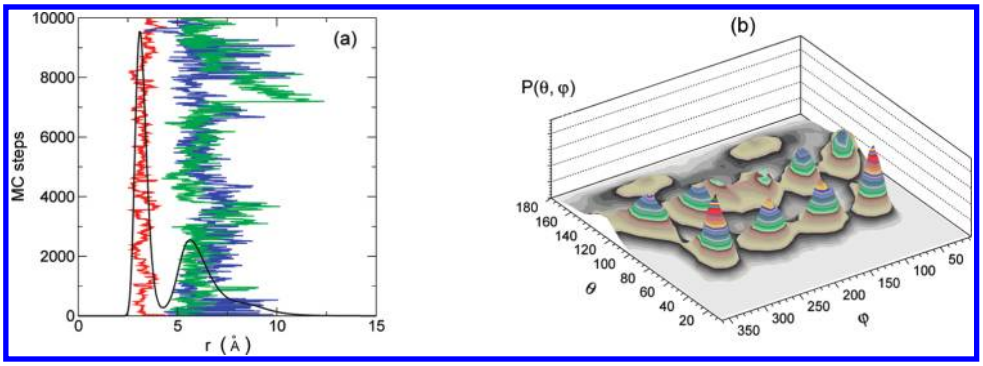


**Figure 7.** (a) Monte Carlo evolution of the distance of three $^4$He atoms from a $K^+$ ion, started at different radial distances from the ion in a droplet with $N = 64$ $^4$He atoms. The radial density profile (black) in arbitrary units is also shown. The distance is monitored at a fixed time-slice. (b) Angular correlations, $P(\theta,\varphi)$, among $^4$He atoms inside the first spherical shell around a $K^+$ ion in a $^4$He droplet with $N = 64$ $^4$He atoms: $\theta \in [60°,78°]$.

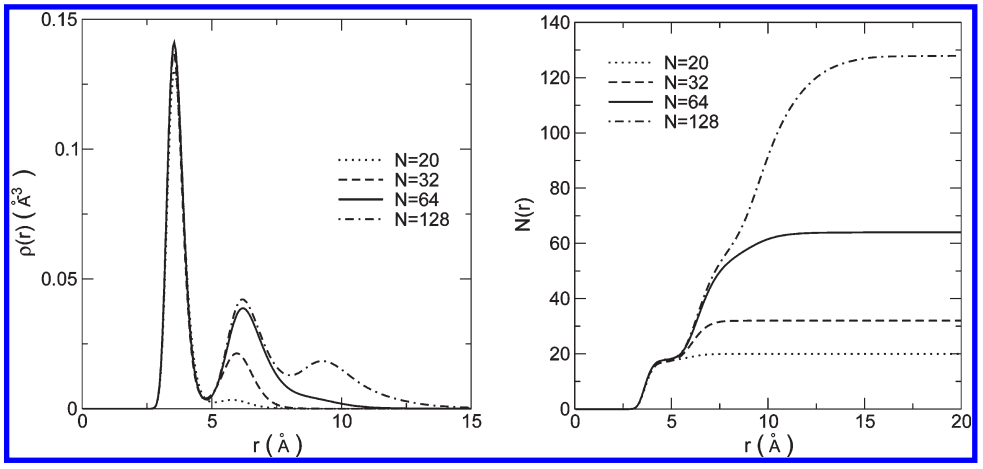


**Figure 8.** Radial $^4$He density $\rho(r)$ and number of atoms $N(r)$ within a sphere of radius $r$ around a $Cs^+$ ion for droplets with different number, $N$, of $^4$He atoms.

There is a lower stability in the number of $^4$He atoms belonging to the first shell as opposed to the $Na^+$ case; also the minimum in the density profile among the first and the second modulation is higher with respect to the $Na^+$ case. This seems to indicate the absence of a particular matching between the ion's size and the interaction potentials but also a higher probability of exchanges or substitutions among $^4$He atoms that belong to the first modulation with those in the second one. We note that 14 or 15 atoms do not correspond to a Platonic solid. In Figure 7a the evolution of the distance of $^4$He atoms from the $K^+$ ion indicates the presence of a higher radial mobility in the second peak of the density profile as opposed to the $Na^+$ case and the absence of solid-like angular correlations. On the contrary, by measuring the function $P(\theta,\varphi)$, angular correlation and solid-like order are still found in the first shell. Taking into account the absence of signal in $P(\theta,\varphi)$ coming from the $^4$He atoms used to define the $z$ axis and the $xz$ plane, the number of peaks in $P(\theta,\varphi)$ is compatible with the number of $^4$He atoms estimated to form the first shell as given by $N(r)$ in Figure 6 (see also $N_1$14 in Table 1 for $N = 64$).

**$Cs^+$-Doped Nanodroplets.** The density profiles of $^4$He atoms around a $Cs^+$ ion in doped nanodroplets with different number, $N$, of $^4$He atoms are shown in Figure 8. $N(r)$ for the smallest nanodroplet shown in Figure 8, $N = 20$, possesses about 17 $^4$He atoms in the first shell, and a small modulation composed, on average, of about 3 $^4$He atoms is also present. The number of atoms in the first shell increases to 18 $^4$He atoms for $N = 64$ and $N = 128$ droplets. This increase is similar to what has been found in $K^+$-doped nanodroplets and, as we have shown also in Table 1, this increase in the number of $^4$He atoms forming the first shell is essentially shared by all the other cases studied here except for the very stable $Na^+$ case. By looking at the Monte Carlo evolution of the radial distance from the $Cs^+$ ion shown in Figure 9a, one can see that, as in the $K^+$ case, the second peak is characterized by $^4$He atoms with a high radial mobility, and solid-like angular correlations are not present. In Figure 9a, it is possible to also see a $^4$He atom moving from the first to the second shell. It is worth noting that for each atom that moves from the first shell to the second there is always a second atom that performs the inverse jump, so these radial exchanges do not destroy or modify the angular and the solid order. This angular and solid order in the first shell is, in fact, evidenced in the angular correlations shown in Figure 9b; also, in this case, the number of visible peaks in $P(\theta,\varphi)$ is compatible with the number of atoms in the first shell, $N_1$18 (see Table 1 for the $Cs^+$ case with $N = 64$ or $N(r)$ in Figure 8).

**$Be^+$-Doped Nanodroplets.** The density profiles of $^4$He atoms around a $Be^+$ alkali-earth ion in doped nanodroplets with different number, $N$, of $^4$He atoms are shown in Figure 10. With regard to the first shell, these density profiles are characterized by

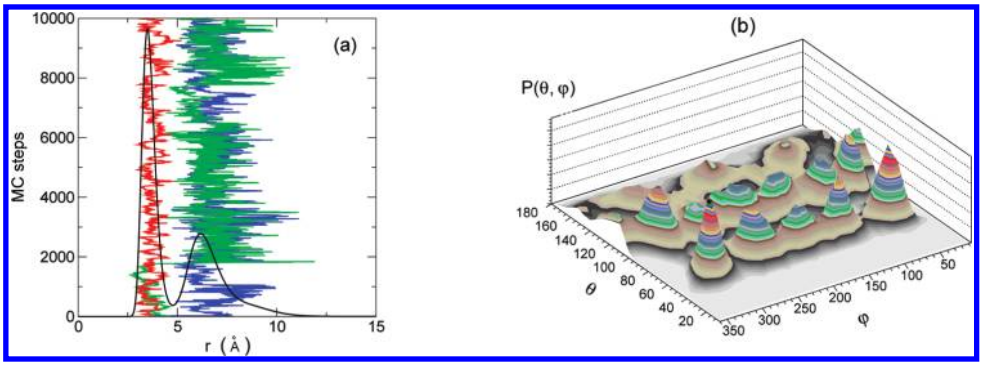


**Figure 9.** (a) Monte Carlo evolution of the distance of three $^4$He atoms from a $Cs^+$ ion, started at different radial distances from the ion in a droplet with $N = 64$ $^4$He atoms. The radial density profile (black) in arbitrary units is also shown. The distance is monitored at a fixed time-slice. (b) Angular correlations, $P(\theta,\varphi)$, among $^4$He atoms inside the first spherical shell around a $Cs^+$ ion in a $^4$He droplet with $N = 64$ $^4$He atoms: $\theta \in [60°,78°]$.

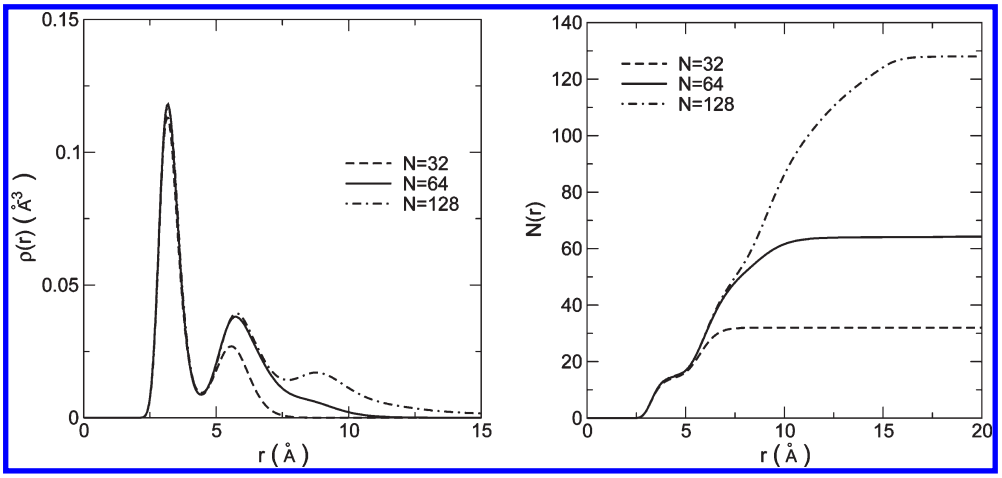


**Figure 10.** Radial $^4$He density $\rho(r)$ and number of atoms $N(r)$ within a sphere of radius $r$ around a $Be^+$ ion for droplets with different number, $N$, of $^4$He atoms.

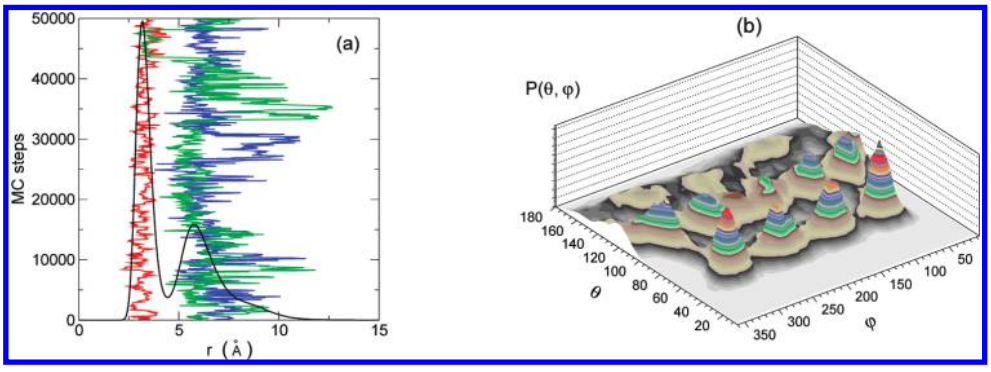


**Figure 11.** (a) Monte Carlo evolution of the distance of three $^4$He atoms from a $Be^+$ ion, started at different radial distances from the ion in a droplet with $N = 64$ $^4$He atoms. The radial density profile (black) in arbitrary units is also shown. The distance is monitored at a fixed time-slice. (b) Angular correlations, $P(\theta,\varphi)$, among $^4$He atoms inside the first spherical shell around a $Be^+$ ion in a $^4$He droplet with $N = 64$ $^4$He atoms: $\theta \in [60°,78°]$.

a lower and larger peak with respect to the alkali ion cases; moreover, a higher local density minimum between the first and the second modulation in the density profiles is present. As stated above, the former property is due to the helium−alkali-earth ion potential interactions, which are less steep at low distances (see Figure 1); the position of the minimum in the potential interaction among a $Be^+$ alkali-earth ion and the $^4$He atoms is similar to the $K^+$ case. This is at the origin of a similar number of $^4$He atoms found in the first shell around the ion, a result already observed with the variational study in ref 15. Also the radial mobility of $^4$He atoms around the ion is similar to the $K^+$ case (see Figure 11a). The analysis of the angular correlations in the first shell (see Figure 11b) reveals the presence of solid-like order and a number of peaks compatible with the expected average number of atoms in this shell given by $N(r)$, i.e., $N_1 = 15$ for $N = 64$ (see Table 1).


dx.doi.org/10.1021/jp200617a |J. Phys. Chem. A 2011, 115, 7300–7309

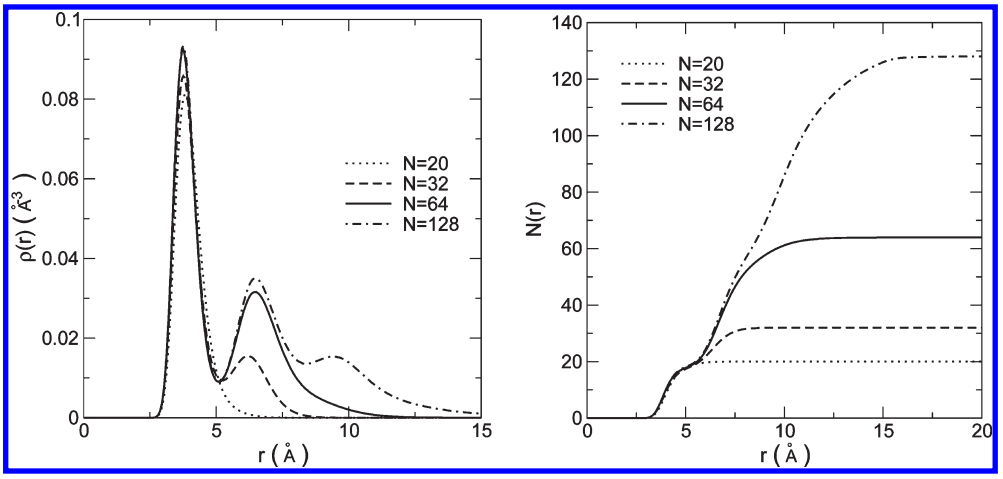


**Figure 12.** Radial $^4$He density $\rho(r)$ and number of atoms $N(r)$ within a sphere of radius $r$ around a $Mg^+$ ion for droplets with different number, $N$, of $^4$He atoms.

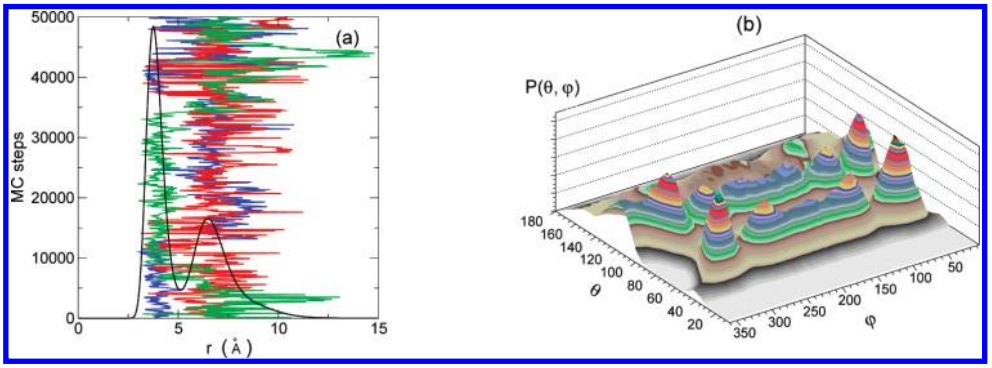


**Figure 13.** (a) Monte Carlo evolution of the distance of three $^4$He atoms from a $Mg^+$ ion, started at different radial distances from the ion in a droplet with $N = 64$ $^4$He atoms. The radial density profile (black) in arbitrary units is also shown. The distance is monitored at a fixed time—-slice. (b) Angular correlations, $P(\theta,\varphi)$, among $^4$He atoms inside the first spherical shell around a $Mg^+$ ion in a $^4$He droplet with $N = 64$ $^4$He atoms: $\theta \in [60°,78°]$.

**$Mg^+$-Doped Nanodroplets.** Nanodroplets doped with one $Mg^+$ ion have the density profile shown in Figure 12. The $Mg^+$—He interaction potential is the shallowest among those studied here. The peak of the first shell, even if well above the freezing density, is smaller than the previous cases. The density profile for the case $N = 20$ consists of a single radial density peak with a small tail at larger distances. By increasing the number of $^4$He atoms in the nanodroplets, a well-defined second modulation in the density profile appears; the first shell consists of about 18 $^4$He atoms, which is similar to the $Cs^+$ case; note also that these two cases correspond to a similar position of the minimum of the ion—He interaction potential. The density minimum between the first and the second modulation in the density profile is similar to the $Be^+$ case, but the analysis of the Monte Carlo evolution of the radial distances of $^4$He atoms from the ion reveals a high probability for the $^4$He atoms to change the shell to which they belong (see Figure 13a); $^4$He atoms are seen to visit all the modulation in the radial density profiles in a few thousand Monte Carlo steps. The analysis of the angular correlations, $P(\theta, \varphi)$, in the first shell indicates the presence of solid-like order, but peaks are wider and overlapping, making more difficult their identification with respect to the other cases (see Figure 13b). $Mg^+$ in a $^4$He droplet has been studied at $T = 0$ K with PIGS,[18] and the authors concluded that the structure in the first shell around the ion is liquid-like. We note that the definition of solid order for systems with such a limited number of atoms can be ambiguous, and it is possible that different definitions or different methods of analysis may lead to different conclusions. In the literature it has been suggested that $Mg^+$ forms a bubble and not a snowball.[26] From our computation we confirm that $Mg^+$ also forms a snowball as was found in ref 15. However, the radial localization of the $^4$He atoms around $Mg^+$ is significantly smaller than those around the other ions, and the exchanges between shells are very frequent, as can be seen in Figure 13a. Due to this high exchange probability it could be interesting to measure, in the future, the local superfluid density inside and outside this snowball to see if such high mobility in the presence of solid-like order could be coupled with a nonzero local superfluid fraction.

## CONCLUSIONS

In summary, we have performed PIMC calculations for alkali and alkali-earth ion-doped $^4$He nanodroplets at low temperatures.

We find that the solid structure around the ion depends on the position of the minimum of the ion—He potential, whereas the degree of localization is a function of the depth of this minimum. For example, by comparing the $K^+$ and $Be^+$ snowballs, or the $Cs^+$ and $Mg^+$ snowballs, because their potential minimum positions are about the same, they have a similar number of particles in the first shell (see Table 1) and a very similar angular

structure, but because the depth of the potential minimum differs, the $^4$He atoms show a very different degree of localization. From the analysis of the evolution of the distances between $^4$He atoms and the ion in the nanodroplet, we have deduced that, even if $^4$He atoms in the first shell are radially localized, exchanges between different shells in the nanodroplet are possible. An interesting question is whether these atoms participate in superfluidity. Of the studied ions, $Na^+$ is the one with the most pronounced local order and this is presumably due to the good match between the minimum positions of the He−He and He−$Na^+$ potentials. We find that for $Na^+$, which has the deepest potential minimum among the studied ions, the snowball has a very pronounced local order both in the first and in the second modulations of the density profile; the angular structure of $P(\theta,\varphi)$ is the only one compatible with a platonic solid within the ions studied, and it is compatible with an icosahedral geometry for the first and the third solid shells, and a dodecahedral geometry for the second solid shell, with a strong angular correlation between shells. Such extended local solid order is remarkable and suggests the presence of particularly strong magic shell effects for the $Na^+$ ion.

It will be interesting in the future to calculate local superfluid densities around the ions, especially to measure the local superfluid density in the shells where solid-like order is present. The present results, obtained with an exact numerical method, confirm previous variational[13−15] and PIGS studies[18] where it was found that the snowball depends very much on the ion both in terms of local order and degree of localization.

## AUTHOR INFORMATION

**Corresponding Author**
*E-mail: Davide.Galli@unimi.it.

## ACKNOWLEDGMENT

We acknowledge useful discussions with E. W. Draeger. This work has been supported by the Italian project "Quantum Fluids and Solids in Confined Geometries" of MIUR.

## REFERENCES

(1) Toennies, J. P.; Vilesov, A. F. *Annu. Rev. Phys. Chem.* **1998**, *49*, 1.
(2) Callegari, C.; Lehmann, K. K.; Schmied, R.; Scoles, G. *J. Chem. Phys.* **2001**, *115*, 10090.
(3) Döppner, T.; Diederich, Th.; Tiggesbäumker, J.; Meiwes-Broer, K.-H. *Eur. Phys. J. D* **2001**, *16*, 13.
(4) Döppner, T.; Diederich, Th.; Göde, S.; Przystawik, A.; Tiggesbäumker, J.; Meiwes-Broer, K.-H. *J. Chem. Phys.* **2007**, *126*, 244513.
(5) Stienkemeier, F.; Mende, S. *Rev. Sci. Instrum.* **2003**, *74* (9), 4071.
(6) Tiggesbäumker, J.; Stienkemeier, F. *Phys. Chem. Chem. Phys.* **2007**, *9*, 4748.
(7) Müller, S.; Mudrich, M.; Stienkemeier, F. *J. Chem. Phys.* **2009**, *131*, 044319.
(8) da Silva, F. F.; Waldburger, P.; Jaksch, S.; Mauracher, A.; Denifl, S.; Echt, O.; Märk, T. D.; Scheier, P. *Chem.—Eur. J.* **2009**, *15*, 7101.
(9) Theisen, M.; Lackner, F.; Ernst, W. E. *Phys. Chem. Chem. Phys.* **2010**, *12*, 14861.
(10) Careri, G.; Scaramuzzi, F.; Thomson, J. O. *Nuovo Cimento* **1959**, *13*, 186.
(11) Reif, F.; Meyer, L. *Phys. Rev.* **1960**, *119*, 1164.
(12) Atkins, K. P. *Phys. Rev.* **1959**, *116*, 1339.
(13) Buzzacchi, M.; Galli, D. E.; Reatto, L. *Phys. Rev. B* **2001**, *64*, 094512.
(14) Galli, D. E.; Buzzacchi, M.; Reatto, L. *J. Chem. Phys.* **2001**, *115*, 10239.
(15) Rossi, M.; Verona, M.; Galli, D. E.; Reatto, L. *Phys. Rev. B* **2004**, *69*, 212510.
(16) Ceperley, D. M. *Rev. Mod. Phys.* **1995**, *67*, 279.
(17) Nakayama, A.; Yamashita, K. *J. Chem. Phys.* **2000**, *112*, 10966.
(18) Paolini, S.; Ancilotto, F.; Toigo, F. *J. Chem. Phys.* **2007**, *126*, 124317.
(19) Coccia, E.; Bodo, E.; Marinetti, F.; Gianturco, F. A. *J. Chem. Phys.* **2007**, *126*, 124319.
(20) Bodo, E.; Coccia, E.; López-Durán, D.; Gianturco, F. A. *Phys. Scr.* **2007**, *76*, C104.
(21) Coccia, E.; Bodo, E.; Gianturco, F. A. *Europhys. Lett.* **2008**, *82*, 23001.
(22) Ahlrichs, R.; Bohm, H. J.; Brode, S.; Tang, K. T.; Toennies, J. P. *J. Chem. Phys.* **1988**, *88*, 6290.
(23) Koutselos, A. D.; Mason, E. A.; Viehland, L. A. *J. Chem. Phys.* **1990**, *93*, 7125.
(24) Bellert, D.; Beckenridge, W. H. *Chem. Rev.* **2002**, *102*, 1595.
(25) Aziz, R. A.; Janzen, A. R.; Moldover, M. R. *Phys. Rev. Lett.* **1995**, *74*, 1586.
(26) Foerste, M.; Guenther, H.; Riediger, O.; Wiebe, J.; Putlitz, G. *Z. Phys. B* **1997**, *104*, 317.